



Estimation of model parameters and simulation of earthquake ground motion by stochastic finite-fault modelling based on a modified slip-related corner frequency

Pengfei Dang^{1,2} · Jie Cui¹ · Qifang Liu³

Accepted: 28 September 2023 / Published online: 13 October 2023

© The Author(s), under exclusive licence to Springer-Verlag GmbH Germany, part of Springer Nature 2023

Abstract

On May 21, 2021, at 21:48 local time, an earthquake with a moment magnitude of 6.1 occurred in Yangbi County, Yunnan Province, China. By using the robust strong ground motion data released by the Yunnan Earthquake Agency, we selected five near-field stations ($R < 100$ km) and determined model parameters, such as the duration, spectral attenuation, stress drop, and site amplification factors of the 2021 Mw 6.1 Yangbi earthquake in China. These model parameters required for the simulation were fed into a stochastic finite-fault model of the corner frequency associated with a dislocation. The modified stochastic finite-fault method was applied to simulate the acceleration recordings of these five near-fault stations, and the acceleration response spectra and Fourier acceleration spectrum were obtained. Comparative observation results reveal that the key input parameters extracted from a few stations and the revised approach established in the current study can adequately predict the near-fault ground motion at high frequencies of the Yangbi earthquake and can demonstrate the contribution of areas with large slips to radiated energy. The proposed method can provide a basis for postdisaster rescue and seismic building design for this region.

Keywords Stochastic finite-fault modelling · Site effect · Corner frequency · Source spectrum · Yangbi earthquake

1 Introduction

Near-fault ground motion recording is of great significance for studying focal mechanisms and ground motion attenuation laws. On the one hand, because the basic characteristics,

generation mechanism, and spatial distribution pattern of near-field ground motion are closely related to the earthquake rupture process, the study of near-field ground motion can provide a theoretical basis for seismological research (Bolt 1973; Yang et al. 2021). On the other hand, by analysing actual strong-motion observation recordings, we can understand the engineering characteristics of ground motion and obtain reasonable ground motion input for seismic design (Takizawa and Jennings 1990).

On May 21, 2021, a Mw 6.1 earthquake in Yangbi, China, occurred at the western boundary of the Sichuan-Yunnan block in the southeastern Tibetan Plateau. The complex tectonic deformations in the area are characterized by large-scale eastwards compression of the plateau materials (Wang and Shen 2020; Liu et al. 2022). It has been reported that the 2021 Mw 6.1 Yangbi, China, earthquake underwent a typical foreshock–mainshock–aftershock sequence (Chen et al. 2022; Zhang et al. 2021; Liu et al. 2022). Based on the report of the China Earthquake Networks Center, the epicentre (25.67°N, 99.87°E) was approximately 9 km away from Yangbi County, and the focal depth was 8 km. After the

✉ Pengfei Dang
iempengfeid@gzhu.edu.cn

✉ Jie Cui
jcui@gzhu.edu.cn

Qifang Liu
qifang_liu@126.com

¹ School of Civil Engineering, Guangzhou University, No.230 Waihuan West Road, Guangzhou 510006, Guangdong Province, China

² Earth System Science Programme, The Chinese University of Hong Kong, Shatin, Hong Kong, China

³ School of Civil Engineering, Suzhou University of Science and Technology, No.1701 Binhe Road, Suzhou 215011, Jiangsu Province, China

earthquake, the results of the seismic macro-intensity map released by the Yunnan Earthquake Agency revealed that the maximum intensity of this earthquake was VIII, in which, most houses were moderately damaged and the structures were damaged and required repair (China Seismic Intensity Scale). Preliminary research results claim that the 2021 Mw 6.1 Yangbi earthquake occurred on a NW–SE right rotating strike-slip secondary fault located on the west side of the Weixi-Qiaohou Fault in the northern section of the Honghe Fault (Qiang et al. 2021). The Honghe Fault is the southwest boundary of the Qinghai-Tibet Plateau, which is the boundary zone of collision and compression between the Indian and Eurasian plates. The Sichuan-Yunnan rhombic block is the most active in the southeast margin of the Qinghai-Tibet Plateau. As of May 22, three people had died, 28 people had been injured, and 192 houses had collapsed. The Yunnan strong-motion network obtained 25 sets of strong-motion observation recordings during the Yangbi earthquake, and only five records were collected at stations located within 100 km of the epicentre. The maximum peak ground acceleration (PGA) was recorded by the Yangbi (053YBX) station, which is approximately 8 km from the epicentre. The PGAs of the EW, NS, and UD components were 379.9, 720.3, and 448.4 cm/s², respectively. Strong ground motion field simulation is essential for determining the disaster scope and earthquake damage intensity (Zhou et al. 2021). Stochastic finite-fault modelling based on dynamic corner frequency (EXSIM), which was proposed by Motazedian and Atkinson (2005), has been demonstrated to be a widely used tool for synthesizing near-field strong ground motions (Mittal et al. 2016; Sun et al. 2018; Karagoz et al. 2018; Mir and Parvez 2020; Dang et al. 2021). However, it is found that the corner frequency used in EXSIM is related only to the rupture sequence of the subfault. The corner frequency of the subfault where the fracture initiation point is located is higher than that of other subfaults, with the expansion of the fracture, the corner frequency of the subfault gradually decreases (Dang et al. 2022a). Moreover, the stress drop of each subfault is considered to be constant. To ensure that the change in the trend of the corner frequency is matched with the real ground motion characteristics, the stress parameter and corner frequency are modified by taking into account the influence of the slip amount on the rupture fault (Dang et al. 2022b). In the current study, the modified EXSIM combined with the slip-related stress drop given by Dang et al. (2022b) was adapted to generate the records of the five near-fault stations of the Yangbi earthquake, and the PGA distribution of the ground motion field near the epicentre was also predicted.

2 Method and data

2.1 Simulation method

The initial finite-fault simulation model (FINSIM) was developed by Beresnev and Atkinson (1997, 1998). In the time domain, the ground motion estimated by all subfaults is superimposed with an appropriate time delay to compute the ground motion caused at the site:

$$a(t) = \sum_{i=1}^{nl} \sum_{j=1}^{nm} a_{ij}(t + \Delta t_{ij}) \quad (1)$$

in which nl and nm indicate the counts of subfaults along the main fault strike (length) and dip (width), respectively; then, the total number of subfaults N can be defined as the product of nl and nm ; Δt_{ij} indicates the time delay of the ground motion simulated by the i th subfault at the j th site point relative to the ground motion generated at the site point at the initiation point, and a_{ij} represents the acceleration waveforms of the ij th subfault.

In EXSIM, the corner frequency of the ij th subfault is defined as a function of time and can be expressed as $f_{0ij}(t) = 4.9 \times 10^6 \beta [\Delta \sigma / (N(t)M_{0ave})]^{1/3}$, where β represents the S-wave velocity (km/s), $N(t)$ indicates the total number of ruptured subfaults on the ruptured fault at time t , M_{0ave} represents the average seismic moment that can be represented as $M_{0ave} = M_0/N$ (unit: dyne.cm = 10^{-7} Nm, Wang et al. 2018), M_0 denotes the seismic moment of the main rupture plane, and $\Delta \sigma$ represents the stress drop in the ω^2 source model (bars, where 10 bars = 1 MPa). The dynamic corner frequency in EXSIM shows that as more subfaults on the ruptured fault are triggered, the corner frequency of the subfault shows a decreasing trend, which cannot correctly describe the rupture process of an earthquake. The results calculated by EXSIM show that the dynamic corner frequency of the subfault where the initiation point is located is always significantly larger than that of the subfaults located elsewhere. The corner frequency of the subfault depends only on the rupture sequence of the subfault, which is inconsistent with the real characteristics of the earthquake rupture process. In this simulation, the following equation was used to obtain the subfault corner frequency (Dang et al. 2020, 2022b):

$$f_{cij} = 7.12 \times 10^6 V_r \left(\frac{N \cdot \Delta \sigma_{ij}}{M_0} \right)^{1/3} \quad (2)$$

where $\Delta \sigma_{ij}$ is the slip-related stress drop of the ij th subfault, which can be written as follows (Dang et al. 2022b):

$$\Delta\sigma_{ij} = \Delta\sigma \cdot \frac{D_{ij}}{\sum_{i=1}^{nl} \sum_{j=1}^{nm} D_{ij}} \tag{3}$$

where D_{ij} denotes the slip value of the ij th subfault, and the modified corner frequency can reflect the uneven slip distribution on the large rupture fault and provide the corner frequency related to the rupture velocity.

Boore (2009) modified this factor to be obtained by the squared of the acceleration spectra and revised the duration to $1/f_0$, thus widening the application range of EXSIM. The scaling factor is expressed as follows:

$$H_{ij} = \sqrt{\frac{N \sum \left\{ f^2 / \left[1 + (f/f_0)^2 \right] \right\}^2}{\sum \left\{ f^2 / \left[1 + (f/f_{0ij})^2 \right] \right\}^2}} \tag{4}$$

in which N indicates the number of all subfaults, and f_0 represents the static corner frequency expressed as $f_0 = 4.9 \times 10^6 \beta (\Delta\sigma/M_0)^{1/3}$ (Boore 1983, 2003).

Further analysis indicated that the corner frequency should be directly associated with the rupture velocity, which strongly affects the corner frequency (Wang 2017; Dang et al. 2020). In EXSIM, changing the rupture velocity does not affect the corner frequency. To solve this problem, Wang (2017) determined the static corner frequency in the form of $f_c = 7.12 \times 10^6 V_r (\Delta\sigma/M_0)^{1/3}$, where V_r represents the rupture velocity in km/s.

A mathematical model was used to incorporate directivity effects (Mavroeidis and Papageorgiou 2003; Motazedian and Moinfar 2006), which had been selected as an option in EXSIM (Boore 2009). However, the mathematical model was not considered because the input parameters were not sufficiently tested.

2.2 Ground-motion data

After the Yangbi earthquake, only five stations within 100 km of the epicentre recorded 25 strong-motion records in the Yunnan Strong Motion Network. Figure 1 shows all stations that were triggered in this earthquake. In the current study, the method proposed by Boore (2001) was used to process the recordings. After baseline correction, the cosine window was used at the start and end of the extracted S-waveform, and the Butterworth bandpass filter (0.08–30 Hz) was used to process the records. The relevant parameters are shown in Table 1.

3 Input parameters

3.1 Source model and geometric spreading function

The source model is an important input parameter in EXSIM. The hybrid source model predicted based on finite-fault modelling was used in the earthquake ground motion simulation of the 2021 Mw 6.1 Yangbi earthquake in China (Dang et al. 2023), which is shown in Fig. 2. The figure indicates that the main fault has a size of 10×9 km². In the simulation, the subfaults are sized at 1×1 km².

The geometric spreading function used in this study can be defined as $G(R) = 1/R$ for $R < R_{01}$, $G(R) = 1/R_{01}$ for $R_{01} < R < R_{02}$, and $G(R) = 1/R^{0.5}$ for $R > R_{02}$, in which R_{01} and R_{02} are defined as $1.5D$ and $2.5D$ (D is the thickness of the Earth’s crust), respectively. However, we do not have detailed site information for the study area, and the geometric spreading function defined by Boore (2003) was adopted in this simulation; this function has been widely used in ground motion simulations of other regions in China (Yaghmaei-Sabegh and Tsang 2011; Zafarani et al. 2015; Zhou et al. 2021; Dang et al. 2021; Zhang et al. 2023).

3.2 High-frequency attenuation (κ)

In seismic engineering, κ_0 or f_{max} is usually used to define the spectral attenuation characteristics of FAS at high frequencies ($>f_0$). Anderson and Hough (1984) defined the attenuation of high-frequency spectra as follows:

$$U(f) = U_0 \exp[-\pi\kappa(R)f] \quad f_E \leq f \leq f_X \tag{5}$$

where κ is used to express the spectral attenuation characteristics of FAS. U_0 represents the amplitude related to the earthquake source and propagation path, and R indicates the epicentral distance. f_E and f_X are used to define the lower and upper frequency limits of the linear trend of FAS (Douglas et al. 2010).

Hough and Anderson (1998) obtained an important parameter, κ_0 , based on the empirical relationship between κ and distance R , which represents the attenuation effect of the soft soil layer on the high-frequency spectra a few kilometres below the surface. When calculating the high-frequency spectral delay parameter κ , the frequency bandwidth ($f_E < f < f_X$) should be at least 10 Hz (Ktenidou et al. 2013; Tafreshi et al. 2022) to weaken the impact of local anomalies of FAS on the synthesized results. If the FAS is displayed in the log-lin space, the amplitude spectrum slope of the frequency range with relatively smooth parts is considered, and the amplitude spectrum of one station is obtained using the formula $\kappa = slope/(\pi \log e)$, in which $slope$

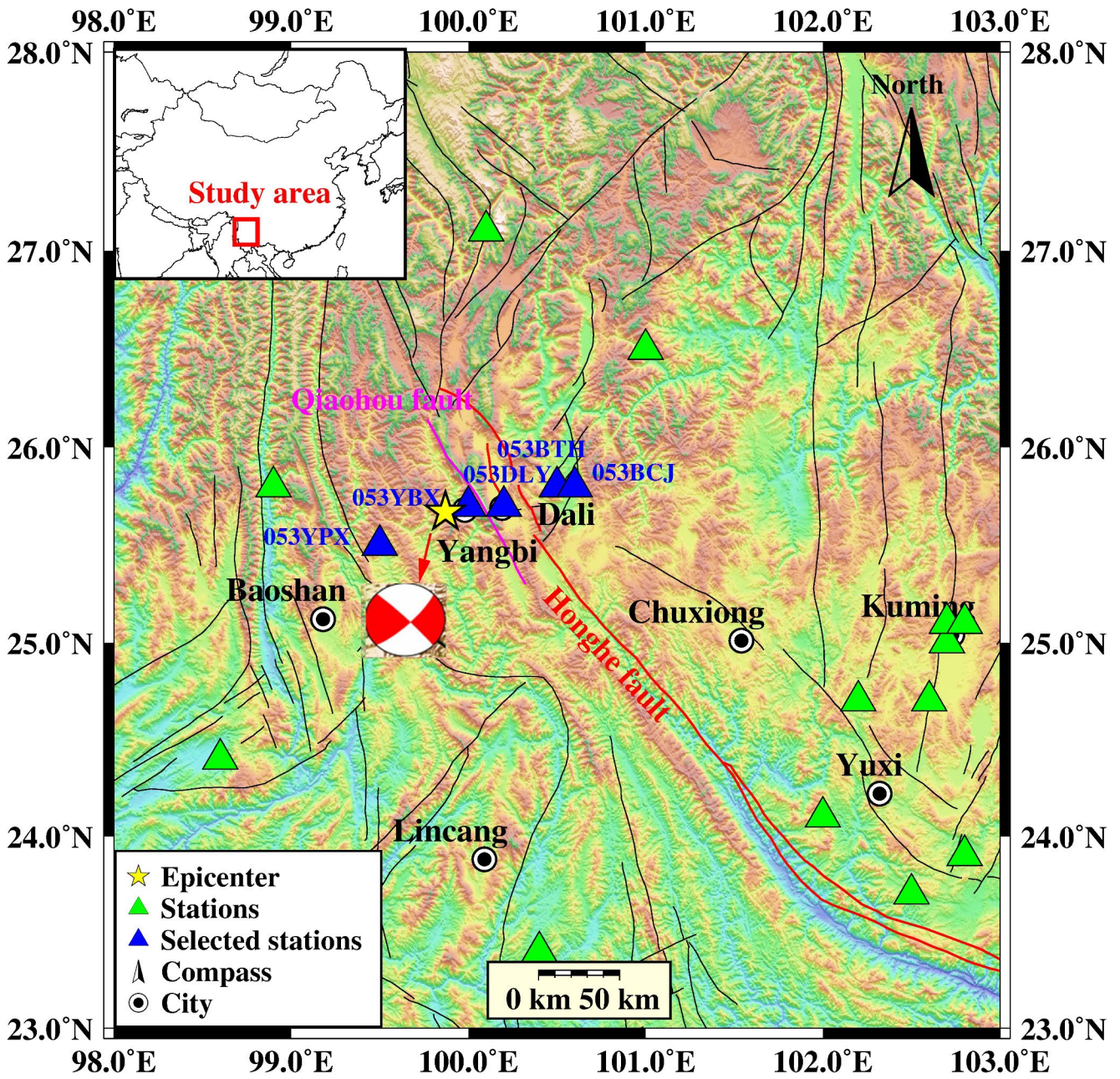


Fig. 1 Distribution of selected stations of the Yangbi earthquake in China. Yellow stars, green triangles and blue triangles represent hypocentres, far-field stations and near-fault stations selected in this study, respectively. The inset map represents the location of the study area in China

Table 1 Information on near-field acceleration observation stations that recorded the Yangbi earthquake

Station	Latitude	Longitude	R	Recorded PGA		Simulated PGA	Site condition
				EW	NS		
053BCJ	25.8	100.6	72	22.5	24.4	26.8	Soil
053BTH	25.8	100.5	66.9	7.2	6.8	7.3	Rock
053DLY	25.7	100.2	31.2	111.5	97.0	95.5	Soil
053YBX	25.7	100.0	7.9	347.6	695.2	267.4	Soil
053YPX	25.5	99.5	41.5	44.6	65.2	72.3	Soil

Note: Unit: PGA, cm/s²; R, Epicentral distance, km; Latitude, °N; Longitude, °E;

The site conditions are obtained from the headerlines of the raw acceleration recordings

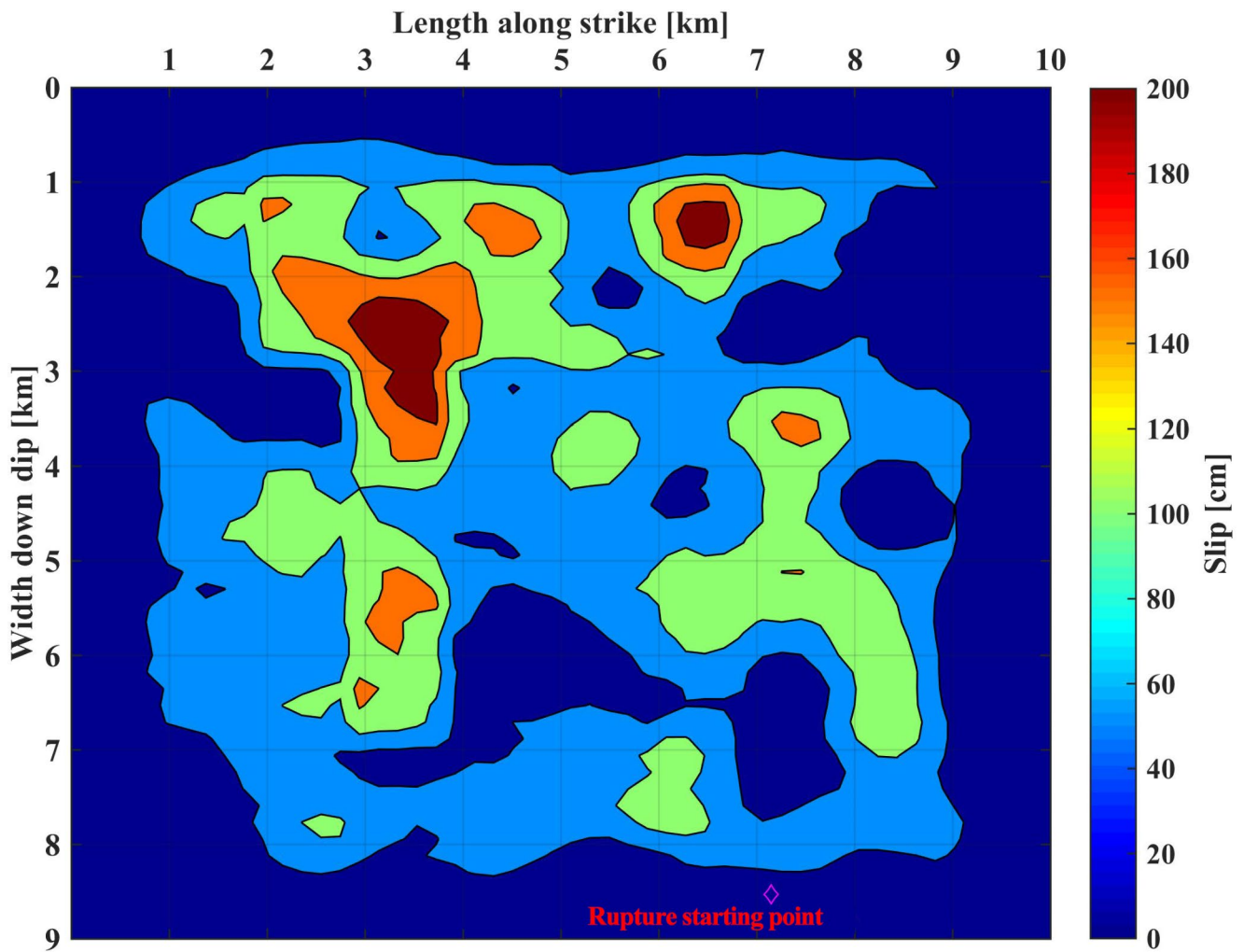


Fig. 2 Slip model of the Yangbi earthquake (Dang et al. 2023). It shows that the main fault has a size of $10 \times 9 \text{ km}^2$. In the simulation, the subfaults are sized at $1 \times 1 \text{ km}^2$, and the maximum slip on the main fault is 2.0 m. The rupture starting point was located at subfault (9, 7)

indicates the slope of the FAS in a given frequency band (f_E and f_X), e represents the natural constant, and \log represents the logarithm. The obtained FAS between 5 and 20 Hz is smoothed using a window function, with a smoothing constant of 20, as defined by Konno and Ohmachi (1998). In the current study, we calculate the value of κ for each station and fit it using the following formula:

$$\kappa = m \cdot R + n \tag{8}$$

in which R indicates the epicentral distance (unit: km), and m and n indicate the model coefficients. In this study, a kappa value of 0.01 was adopted (Zhou et al. 2021).

3.3 Ground-motion duration

The ground-motion duration comprises two parts, i.e., a rise time and a path duration, which can be defined as follows:

$$T_d = T_s + T_p \tag{9}$$

where T_s is the rise time ($T_s = 1/f_0$, f_0 = corner frequency), and T_p is the path duration. Atkinson and Boore (1998) established a four-stage empirical relationship between duration and distance based on strong-motion data obtained in eastern North America. Husid (1969) proposed expressing ground motion energy by the square of acceleration and defined the standardized format of energy (Dabaghi and Kiureghian 2016):

$$I(t) = \frac{\int_0^t a^2(t) dt}{\int_0^T a^2(t) dt} \tag{10}$$

in which T indicates the ground-motion duration; therefore, the upper and lower limits of $I(t)$ are 1 and 0, respectively. Husid (1969) defined the time corresponding to the part where the ground motion energy is between 5% and 95%

as the effective duration ($t_2 - t_1$), which can be expressed as $I(t_1) = 0.05$ and $I(t_2) = 0.95$ (Dang et al. 2022b). In the current study, the effective duration of each ground motion observation record is calculated, and the relationship between the duration and epicentral distance is given by linear fitting: $T(R) = 0.2705R + 4.928$ for EW, and $T(R) = 0.238R + 3.787$ for NS (Fig. 3).

3.4 Site effect

Site conditions are the main factors that affect the amplitude and frequency components of ground motion for the propagation path of seismic waves, which is expressed as follows (Boore 2003):

$$G(f) = A(f) D(f) \quad (11)$$

where $A(f)$ represents the near-surface site amplification factor, $D(f)$ indicates the near-surface attenuation effect at high frequency, and $A(f)$ is related to the crustal velocity gradient and S-wave velocity structure. The application of the site effect in EXSIM was discussed in detail by Dang et al. (2022b) in the 2013 Mw 6.6 Lushan, China earthquake ground motion simulation. The results show that although H/V is not the most appropriate method for calculating site amplification, the H/V estimation results combined with crustal site amplification can enable EXSIM to obtain more accurate simulation results. Since there are no detailed drilling data, we use the horizontal to vertical (H/V) spectral ratio (Lermo and Chavez 1993) to roughly estimate the local site amplification factors of the five observation stations (Roumelioti and Beresnev 2003; Yalcinkaya et al. 2012; Chopra et al. 2012; Toni 2017; Dang et al. 2020, 2022b; Meneisy

et al. 2020), which is shown in Fig. 4. Figure 4 shows that the spectral ratio curve of 053BTH approaches one at most frequency points, which can be roughly judged as a bedrock station, and it is consistent with the site condition results obtained in the header files of the recording. Furthermore, the site amplification functions calculated by the H/V spectral ratio can roughly reflect the site conditions. In addition, the H/V curve at station 053YPX shows multiple peak characteristics, which may be attributed to the existence of multiple impedance interfaces under the surface where the station located or the resonance of the S-wave. In this simulation, the crustal site amplifications for rock and soil sites were given by Boore and Joyner (1997).

3.5 Stress drop

The stress drop is a key parameter in seismic calibration rates. In EXSIM, the stress drop parameter, which mainly affects the level of the high-frequency amplitude spectrum, is close to the concept of static stress drop. Combined with the regional data, we set the stress drop to 1–6 MPa, with an interval of 1 MPa for simulation, and then, we obtained the spectral ratio curve between the predicted and observed acceleration response spectra (PSA) values, as shown in Fig. 5; we set the stress drop with the minimum error between the predicted and observed values as the selected stress drop (Dang et al. 2022b), which indicates that when the stress drop is greater than 20 bars, the effect of the stress drop on the model residual is relatively small. For quality factor Q , we refer to Xu et al. (2010), who used the records of medium, small, and strong earthquakes in Sichuan and Yunnan ($Q = 180f^{0.5}$). According to the crust 1.0 global crustal model, the S-wave velocity in the Yangbi area of

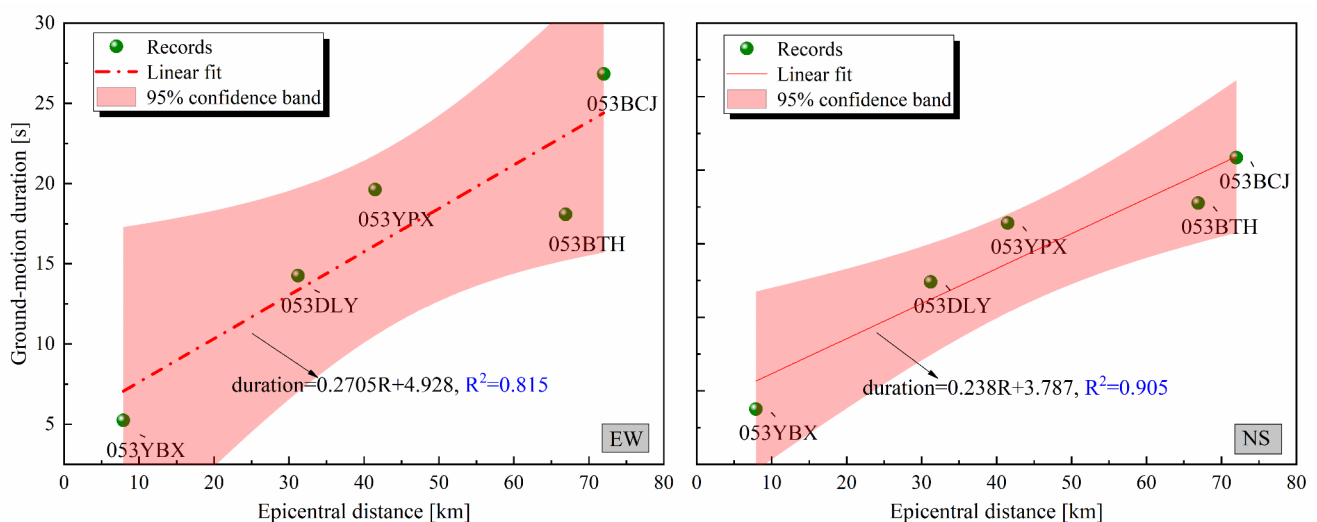


Fig. 3 Ground-motion duration for the EW (left panel) and NS (right panel) components of the 2021 Mw 6.1 Yangbi earthquake. The sphere represents the value obtained by recordings, the red dotted line denotes the linear fitting line, and the filled areas denote the 95% confidence interval

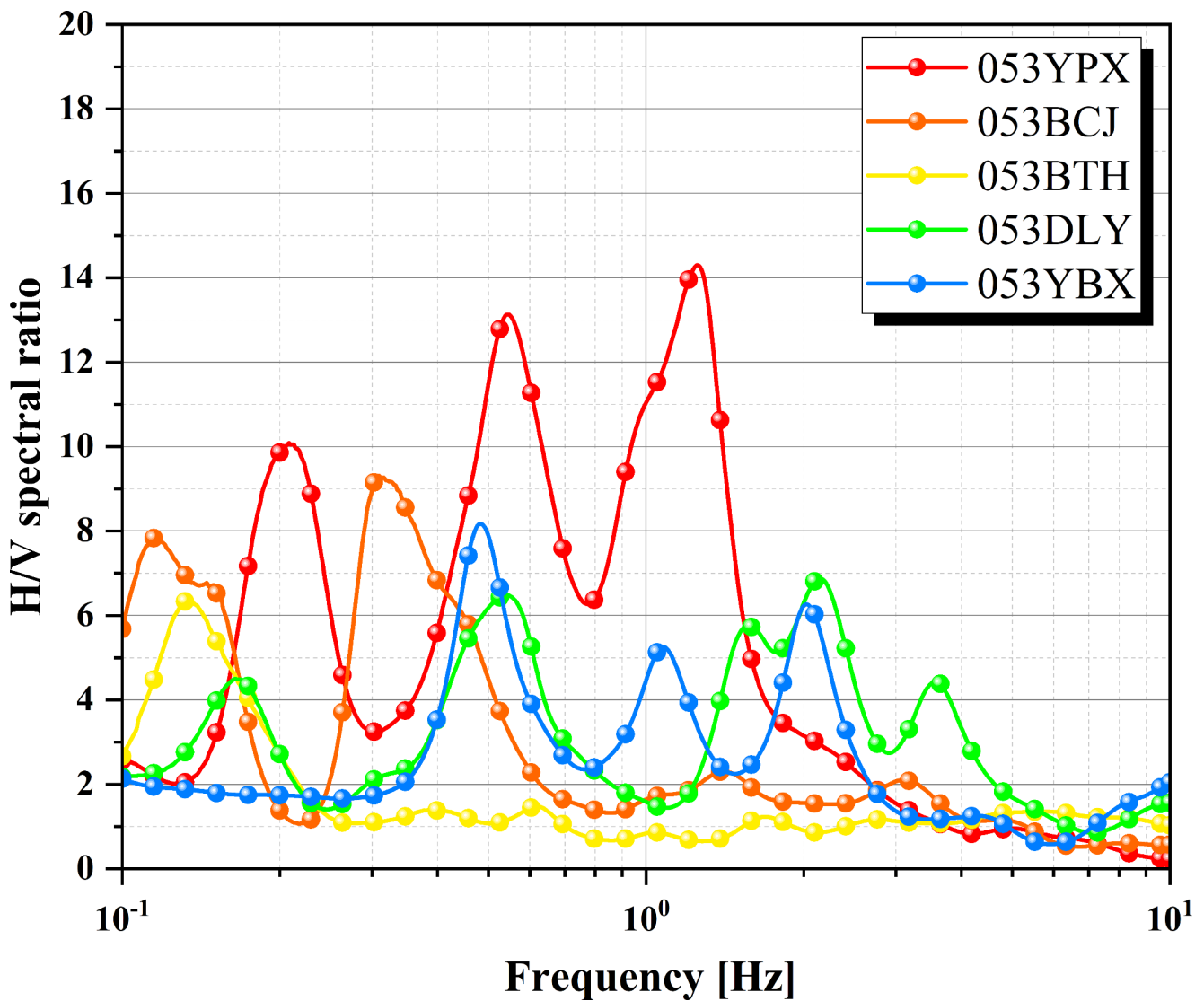
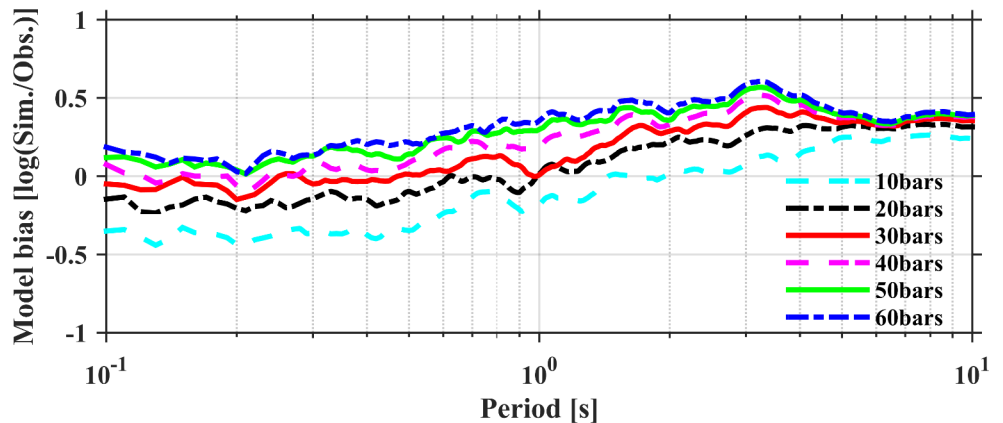


Fig. 4 Local site amplification functions approximately calculated by H/V spectral ratios adopted in the current study. The H/V curve at station 053YPX shows multiple peak characteristics, which may result

from the existence of multiple impedance interfaces under the surface where the station located or the resonance of the S-wave

Fig. 5 Model bias ($\log(\text{Sim./Obs.})$) for different stress drops with respect to periods. The light blue dashed line, black dashed-dotted line, red solid line, magenta dashed line, green solid line and blue dashed-dotted line represent the model residuals calculated when the stress parameters are 10, 20, 30, 40, 50 and 60 bars



Yunnan Province is 3.55 km/s, and the medium density is 2.74 g/cm³ (Qiang et al. 2021). Other parameters are presented in Table 2.

4 Analysis and discussion

4.1 Comparison between simulated and observed values

In this simulation, the model bias was estimated on a logarithmic scale between the simulated and recorded PSAs (Pan et al. 2022; Pezeshk et al. 2022). Combined with the parameters given in Table 2 and the EXSIM based on corner frequency related to dislocation established in the current study, five near-fault observation stations with epicentral distances of < 100 km from the Yangbi earthquake are simulated, and the results are plotted in Fig. 6. The simulated PSA and Fourier amplitude spectrum (FAS) of the stations 053BCJ, 053DLY, and 053YBX are well matched with the recorded values. The synthesized results of stations 053BTH and 053YPX are in good agreement with the recorded values at high frequencies above 1 Hz or short periods less than 1 s, but they are obviously overestimated in low-frequency ($f < 1$ Hz) or long-period ($T > 1$ s) records, which may be

because the selected estimated local site functions cannot correctly represent the real geological conditions of the sites. For station 053YPX, overestimation of low-frequency radiation may be attributed to the strong synthetic source radiation or weak high-frequency attenuation. In addition, EXSIM fails to fully consider the simulation effect on low frequencies. The stochastic simulation method has obvious advantages at high frequencies; thus, the current paper also focuses on the high-frequency ($f > 1$ Hz) simulation results. From the simulated PSA and FAS, the EXSIM revised by Dang et al. (2020) can reconstruct the earthquake ground-motion field of the 2021 Mw 6.1 Yangbi earthquake. The synthetic PGAs of four stations, namely, 053BCJ, 053DLY, 053YPX, and 053BTH, are slightly different from the recorded PGAs, whereas those of the 053YBX station are significantly different from the observed values. Since the epicentral distance of the 053YBX station is only 7.9 km, it may be affected by the fault size.

The distribution of the original dynamic corner frequency and the revised model (the current study) are displayed in Fig. 7, which shows that the dynamic corner frequency is the highest only at the rupture starting point. With the expansion of the rupture area, the corner frequency gradually decreases. The corner frequency of a subfault is related only to the rupture order of the subfault. The corner frequency based on dislocation variation shows the contribution of asperities to radiated energy, which reflects the fact that the corner frequency of a subfault with a large slip is also large.

4.2 Prediction of the PGA distribution

In the current study, the EXSIM revised by Dang et al. (2020) is used to simulate the PGA of 961 virtual points near the epicentre of the Yangbi earthquake (Fig. 8), and the grid accuracy is 0.5°. In the simulation, the model parameters, except for local site amplification, used to simulate the PGA of 961 nodes are listed in Table 2, and the prediction result is only the result of one run. The average H/V ratios of the five selected stations are defined as the local site amplification factors adopted in this section. In this case, the simulated PGAs at the selected near-field stations are 18.9 (053BCJ), 10.6 (053BTH), 90.8 (053DLY), 254.7 (053YBX), and 50.9 cm/s² (053YPX), which are slightly matched with the observed PGAs. Overall, Fig. 8 shows that the predicted and recorded PGAs roughly match the observed values, and the predicted PGA distribution can well describe the characteristics of PGA attenuations with distance. The results show that the recommended model parameters obtained from only a few near-fault stations in this study can reasonably predict certain characteristics of the Yangbi, China, earthquake. However, for station 053DLY, the simulated PGA

Table 2 Input parameters required for simulating the Yangbi earthquake

Parameter	Value	References
Fault orientation (strike, dip)	315°/ 86°	Globe CMT
Depth of top (km)	3.39	Qiang et al. (2021)
Moment magnitude	6.1	Globe CMT
Average stress drop (MPa)	3	This study
Fault dimensions along strike and dip (km)	10 by 9	This study
Sub-fault dimensions (km)	1	This study
Density (g/cm ³) and shear-wave velocity (km/s)	2.74, 3.55	Qiang et al. (2021)
Kappa (s)	0.01	Zhou et al. (2021)
Quality factor	180 ^{0.5}	Xu et al. (2010)
Geometrical spreading	1/R ($R \leq 70$ km), 1/70 (70 km < R ≤ 130 km), 1/R ^{0.5} ($R \geq 130$ km)	Boore (2003)
Duration model	0.238×R + 3.787	This study
Rupture velocity	0.8×(shear-wave velocity)	Motazedian and Atkinson (2005)
Crustal amplification function	Class A for 053BTH Class C for others	Boore and Joyner (1997)
Local site amplification	H/V spectral ratios	This study

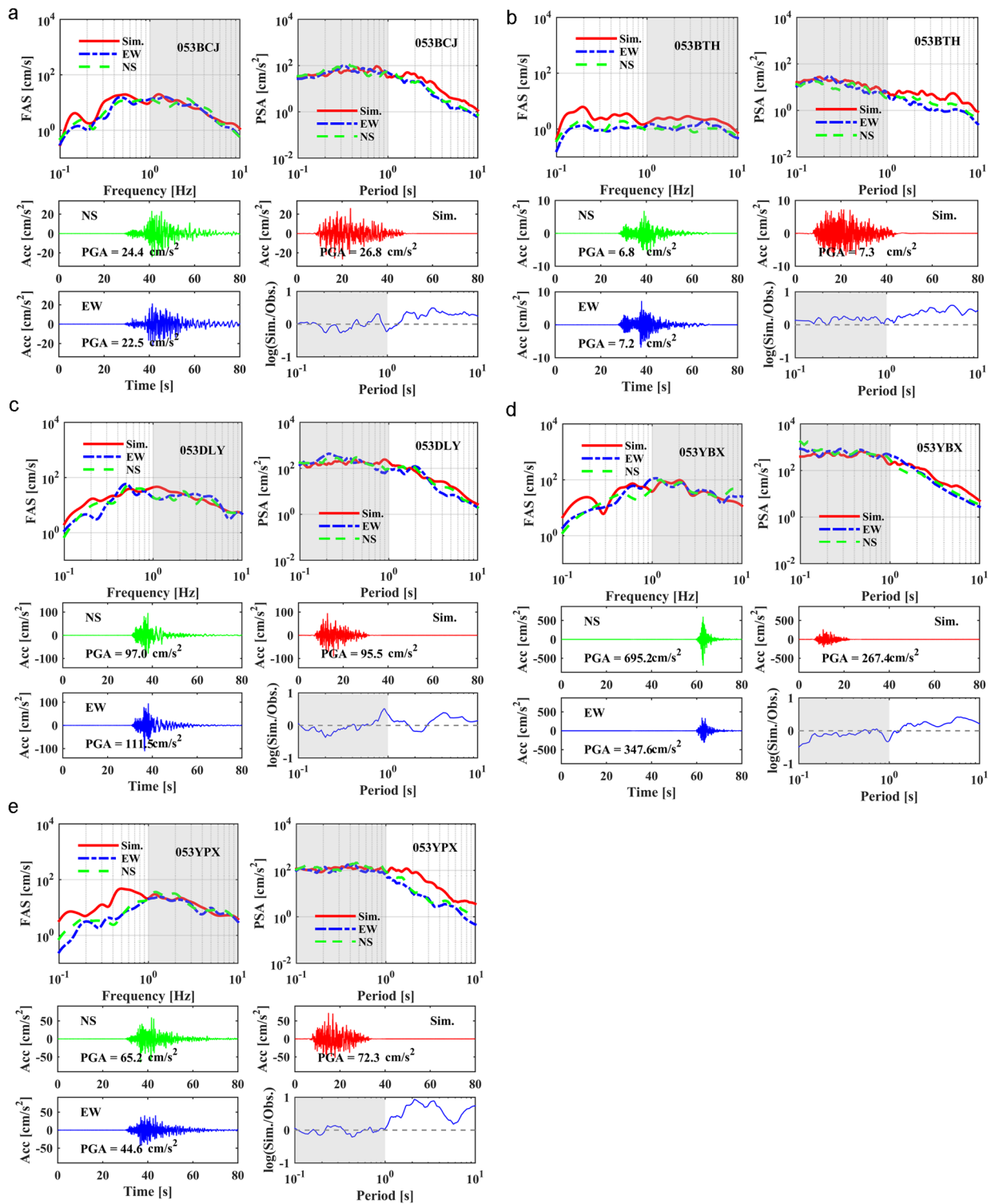


Fig. 6 Comparison of the simulated results and recorded values in terms of the FAS, PSA, and time histories. The solid line (red) represents the simulated value, the dashed line (blue) indicates E–W, the dotted line (green) represents N–S, and the shaded area represents the

frequency (> 1 Hz) or period (< 1 s) range considered in the current study. In this study, the acceleration time history was the result of only one run. The PGA, FAS, and PSA were obtained from the average of 30 runs

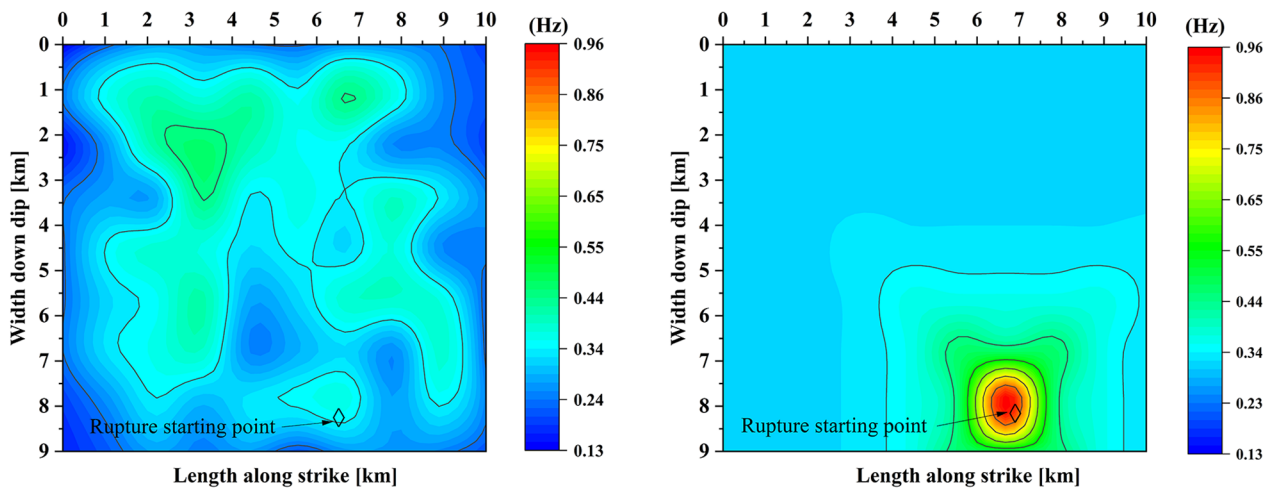
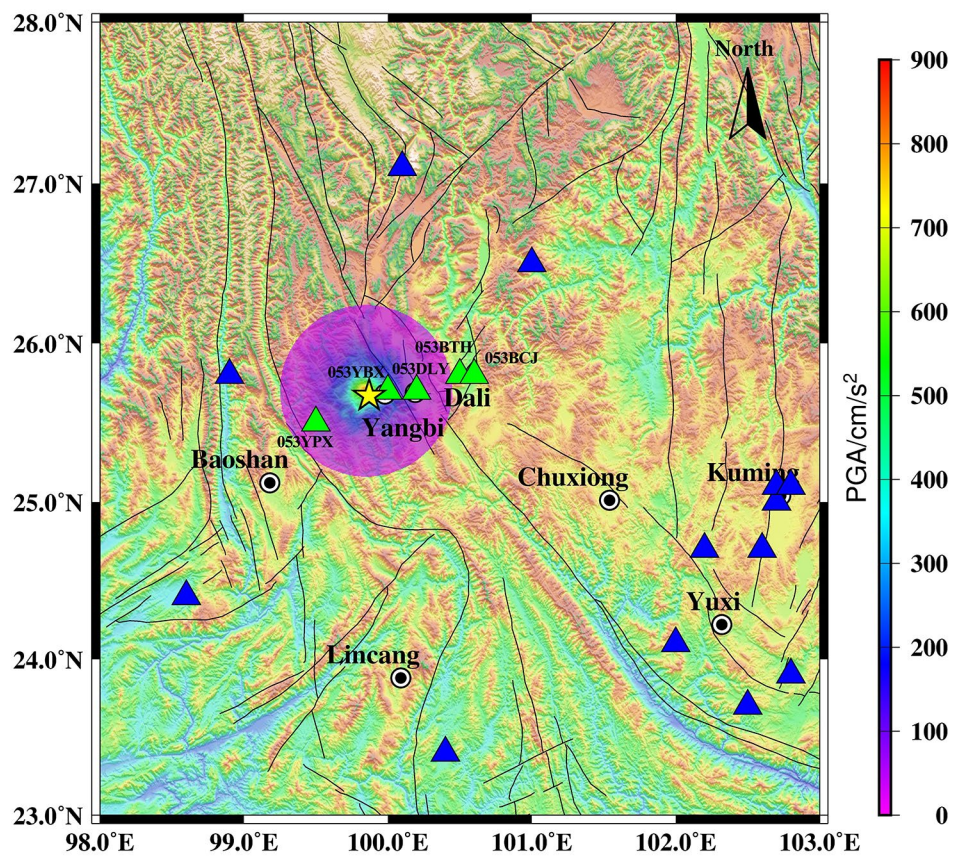


Fig. 7 Corner frequency distribution obtained from the current study (left panel) and EXSIM (right panel). The results obtained from the dynamic corner frequency show that the corner frequency is the largest only at the rupture starting point. With the expansion of the rupture area, the corner frequency gradually decreases, and the subfault corner

frequency is related only to the fault rupture sequence. However, the results obtained from the revised model are related to the slip amount on the rupture plane, which shows the contribution of the asperity body to the radiation energy. The rupture starting point was located at subfault (9, 7)

Fig. 8 Predicted near-field PGA distribution of the Mw 6.1 Yangbi earthquake. In this study, the input parameters, except for local site amplification factors, used to simulate the PGA of 961 nodes are listed in Table 2, and the prediction result is the result of only one run



is slightly smaller than the observed PGA. Moreover, the attenuation law is close to that of circular diffusion, which shows no pronounced directivity or hanging wall effects.

5 Conclusion

The current paper predicts a hybrid slip model of the Yangbi earthquake, and the corner frequency based on dislocation variation is established. The PGA field distribution of five selected stations and 961 virtual points near the epicentre is simulated using the EXSIM model improved by Dang et al. (2020). The main results are presented below:

1. The EXSIM with slip-correlated corner frequency established in the current study can generate the acceleration time series of near-fault observation stations of the Yangbi, China, earthquake, and it is consistent with the observation values in the high-frequency band considered in the study, which adequately demonstrates that the revised corner frequency model can reasonably predict the earthquake ground-motion field of the Yangbi earthquake. The corner frequency based on dislocation can better reflect the contribution of subfaults with large slip to radiated energy, which is consistent with the actual earthquake process.
2. For the predicted near-field PGA distribution, the simulation results of the current study also match well with the observed values, reflecting the attenuation law of PGA with distance.

Although the rupture velocity has a significant impact on the amplitude spectrum of large earthquakes, the improved corner frequency introduced in this study introduces a variable rupture velocity model, making the stochastic finite-fault method more suitable for simulating large earthquakes. However, the rupture velocity is usually difficult to determine, and setting different rupture velocities for each subfault can make the simulation quite complex, which may cause inconvenience in engineering applications.

Overall, EXSIM has significant advantages in high-frequency bands. From the predicted ground motion characteristics, EXSIM, developed by considering slip-related corner frequency can accurately predict the ground-motion field distribution of the Yangbi, China, earthquake, providing a reliable theoretical basis for structural earthquake resistance and postdisaster rescue in this region. The regional model parameters established in the study can also add to the ground motion parameter database of the study area. The estimation methods of these parameters can also provide insights for future studies of areas with less seismic data or the prediction of future earthquakes.

5.1 Data and resources

The EXSIM Fortran program can be downloaded from the website: http://daveboore.com_www.daveboore.com/software_online.html (last accessed March, 2021). Some source parameters are obtained from the Global CMT, <https://www.globalcmt.org/> (last accessed October 2021). The acceleration recording of the 2021 Yangbi earthquake was released by the China Strong Motion Network Center. Data for this study are provided by Institute of Engineering Mechanics, China Earthquake Administration and can be downloaded from National Earthquake Data Center (<https://data.earthquake.cn/datashare/report.shtml?PAGEID=datasourcelist&dt=ff80808277cc56050179c55ee7220005>, last accessed July, 2021) upon reasonable request.

Some plots (Figs. 1 and 9) were made using the Generic Mapping Tools (GMT) software which can be downloaded from the website: <https://www.gmt-china.org/download/> (last accessed May, 2021), and some plots (Figs. 2, 5, 6 and 7, and 8) were made using the MATLAB software which can be downloaded from the website: <https://www.mathworks.cn/campaigns/products/trials.html> (last accessed March, 2016). The other figures were prepared using the Origin software (<https://www.originlab.com/>, last accessed February, 2022).

Acknowledgements The authors would like to express gratitude to Prof. D. Motazedian, the main author of EXSIM, for his valuable comments. Finally, the authors would also like to thank the Editor-in-Chief Andreas Langousis and four anonymous reviewers for their valuable comments.

Author contributions All authors contributed to the study conception and design. Material preparation, data collection and analysis were performed by Pengfei Dang. The first draft of the manuscript was written by Pengfei Dang and all authors commented on previous versions of the manuscript. All authors read and approved the final manuscript.

Funding This work was supported by the National Key Research and Development Program of China (Grant No. 2022YFC3003601), the National Natural Science Foundation for Young Scientists of China (Grant No. 42204050), the Postdoctoral Office of Guangzhou City, China (Grant No. 62216242), the Postdoctoral Program of International Training Program for Young Talents of Guangdong Province, and the National Natural Science Foundation of China (Grant Nos. 52020105002 and 51878192).

Declarations

Competing interests The authors declare no competing interests.

References

- Anderson JG, Hough SE (1984) A model for the shape of the Fourier amplitude spectrum of acceleration at high frequencies. *Bull Seismol Soc Am* 74(5):1969–1993

- Atkinson GM, Boore DM (1998) Evaluation of models for earthquake source spectra in Eastern North America. *Bulletin of the Seismological Society of America* 1998; 88(4): 917–934
- Beresnev IA, Atkinson GM (1997) Modeling finite-fault radiation from the ω^n spectrum. *Bull Seismol Soc Am* 87(1):67–84
- Beresnev IA, Atkinson GM (1998) FINSIM-a FORTRAN program for simulating stochastic acceleration time histories from finite faults. *Seismol Res Lett* 69(1):27–32
- Bolt BA (1973) Duration of strong ground motion. See: *Proceeding of the 5th WCEE, Rome, Italy. 1973; 1: 1304–1313*
- Boore DM (1983) Stochastic simulation of high-frequency ground motion based on seismological models of the radiated spectra. *Bull Seismol Soc Am* 73(6):1865–1894
- Boore DM (2001) Effect of baseline corrections on displacements and response spectra for several recordings of the 1999 Chi-Chi, Taiwan. *Bull Seismol Soc Am* 91(5):1199–1211
- Boore DM (2003) Simulation of ground motion using the stochastic method. *Pure appl Geophys* 160(3):635–676
- Boore DM (2009) Comparing stochastic point-source and finite-source ground-motion simulations: SMSIM and EXSIM. *Bull Seismol Soc Am* 99(6):3202–3216
- Boore DM, Joyner WB (1997) Site amplifications for generic rock sites. *Bull Seismol Soc Am* 87(2):327–341
- Chen JL, Hao JL, Wang Z, Xu T (2022) The 21 May mw 6.1 Yangbi earthquake – a unilateral rupture event with conjugately distributed aftershocks. *Seismol Res Lett* 93(3):1382–1399
- Chopra S, Kumar D, Choudhury P, Yadav RBS (2012) Stochastic finite fault modelling of mw 4.8 earthquake in Kachahh, Gujarat, India. *J Seismolog* 16:435–449
- Dabaghi M, Kiureghian AD (2016) Stochastic model for simulation of near-fault ground motion. *Earthq Eng Struct Dynamics* 46(6):963–984
- Dang PF, Liu QF, Song J (2020) Simulation of the Jiuzhaigou, China, earthquake by stochastic finite-fault method based on variable stress drop. *Nat Hazards* 103(2):2295–2321
- Dang PF, Liu QF, Xia SL, Ma WJ (2021) A stochastic method for simulating near-field seismograms: application to the 2016 Tottori earthquake. *Earth and Space Science* 8(11):e2021EA001939
- Dang PF, Cui J, Liu QF, Xia SL (2022a) Slip-correlated high-frequency scaling factor for stochastic finite-fault modeling of ground motion. *Bull Seismol Soc Am* 112(3):1472–1482
- Dang PF, Cui J, Liu QF (2022b) Parameter estimation for predicting near-fault strong ground motion and its application to Lushan earthquake in China. *Soil Dyn Earthq Eng* 156:107223
- Dang PF, Cui J, Liu QF, Ji LJ (2023) A method for predicting hybrid source model of near-field ground motion: application to Yangbi earthquake in China. *Seismol Res Lett* 94(1):189–205
- Douglas J, Gehl P, Bonilla LF, Gelis C (2010) A κ model for mainland France. *Pure appl Geophys* 167(11):1303–1315
- Hough SE, Anderson JG (1988) High frequency spectra observed at Anza: implications for Q structure. *Bull Seismol Soc Am* 78(2):692–707
- Husid RL (1969) Analisis de terremotos, Analisis general. *Reevista del IDIEM* 8(1):21–42
- Karagoz O, Chimoto K, Yamanaka H, Ozel O, Citak S (2018) Broad-band ground-motion simulation of the 24 May 2014 Gokceada (North Aegean Sea) earthquake (mw 6.9) in NW Turkey considering local soil effects. *Bull Earthq Eng* 16:23–43
- Konno K, Ohmachi T (1998) Ground-motion characteristics estimated from spectral ratio between horizontal and vertical component of microtremor. *Bull Seismol Soc Am* 88(1):228–241
- Ktenidou OJ, Gelis C, Bonilla LF (2013) A study on the variability of kappa (κ) in a borehole: implications of the computation process. *Bull Seismol Soc Am* 83(5):1574–1594
- Lermo J, Chavez GFJ (1993) Site effect evaluation using spectral ratios with only one station. *Bull Seismol Soc Am* 83(5):1574–1594
- Liu XG, Xu WB, He ZL, Fang LH, Chen ZD (2022) Aseismic slip and cascade triggering process of foreshocks leading to the 2021 mw 6.1 Yangbi earthquake. *Seismol Res Lett* 93(3):1413–1428
- Mavroeidis GP, Papageorgiou AS (2003) A mathematical representation of near-fault ground motions. *Bull Seismol Soc Am* 93:1031–1099
- Meneisy AM, Toni M, Omran AA (2020) Soft sediment characterization using seismic techniques at Beni Suef city, Egypt. *J Environ Eng Geophys* 25(3):391–401
- Mir RR, Parvez IA (2020) Ground motion modelling in northwestern Himalaya using stochastic finite-fault method. *Nat Hazards* 103:1989–2007
- Mittal H, Wu YM, Chen DY, Chao WA (2016) Stochastic finite modeling of ground motion for March 5, 2012, mw 4.6 earthquake and scenario greater magnitude earthquake in the proximity of Delhi. *Nat Hazards* 82:1123–1146
- Motazedian D, Atkinson GM (2005) Stochastic finite-fault modeling based on a dynamic corner frequency. *Bull Seismol Soc Am* 95(3):995–1010
- Motazedian D, Moinfar A (2006) Hybrid stochastic finite fault modeling of 2003, M6.5, bam earthquake (Iran). *J Seismolog* 10:91–103
- Pan D, Miura H, Kanno T, Shigefuji M, Abiru T (2022) Deep-neural-network-based estimation of site amplification factor from microtremor H/V spectral ratio. *Bull Seismol Soc Am* 112(3):1630–1646
- Pezeshk S, Farhadi A, Haji-Soltani A (2022) A new model for vertical-to-horizontal response spectral ratios for central and eastern north America. *Bull Seismol Soc Am* 112(4):2018–2030
- Qiang SY, Wang HW, Wen RZ, Li CG, Ren YF (2021) Three-dimensional ground motion simulations by the stochastic finite-fault method for the Yangbi, Yunnan Ms6.4 earthquake on May 21, 2021. *Chin J Geophys* 64(12):4538–4547. <https://doi.org/10.6038/cjg2021P0404> (In Chinese)
- Roumelioti Z, Beresnev IA (2003) Stochastic finite-fault modeling of ground motions from the 1999 Chi-Chi, Taiwan, earthquake: application to rock and soil sites with implications for nonlinear site response. *Bull Seismol Soc Am* 93(4):1691–1702
- Sun JZ, Yu YX, Li YQ (2018) Stochastic finite-fault simulation of the 2017 Jiuzhaigou earthquake in China. *Earth Planets and Space* 70:128
- Tafreshi MD, Bora SS, Ghofrani H, Mirzaei N, Kazemian J (2022) Region- and site-specific measurements of kappa (κ_0) and associated variabilities for Iran. *Bull Seismol Soc Am* 112(6):3046–3062
- Takizawa AH, Jennings PC (1990) College of a model for ductile reinforced concrete frame under extreme earthquake motions. *Earthquake Eng Struct Dynam* 8(2):117–144
- Toni M (2017) Simulation of strong ground motion parameters of the 1 June 2013 Gulf of Suez earthquake, Egypt. *NRIAG J Astron Geophys* 6(1):30–40
- Wang ZY (2017) Research on stochastic method for high frequency of ground motions. Ph. D thesis. Harbin: Institute of Engineering Mechanics, China Earthquake Administration; (In Chinese)
- Wang M, Shen ZK (2020) Present-day crustal deformation of continental China derived from GPS and its tectonic implications. *J Geophys Res* 125(2). <https://doi.org/10.1029/2019JB018774>
- Wang HW, Ren YF, Wen RZ (2018) Source parameters, path attenuation and site effects from strong-motion recordings of the Wenchuan aftershocks (2008–2013) using a non-parametric generalized inversion technique. *Geophys J Int* 212:872–890
- Xu Y, Herrmann RB, Wang CY (2010) Preliminary high-frequency ground-motion scaling in Yunnan and southern Sichuan, China. *Bull Seismol Soc Am* 100(5B):2508–2517
- Yaghmaei-Sabegh S, Tsang HH (2011) An updated study on near-fault ground motions of the 1978 Tabas, Iran, earthquake (mw = 7.4). *Scientia Iranica* 18(4):895–905

- Yalcinkaya E, Pinar A, Uskuloglu O, Tekebas S, Firat B (2012) Selecting the most suitable rupture model for the stochastic simulation of the 1999 Izmit earthquake and prediction of peak ground motions. *Soil Dyn Earthq Eng* 42:1–16
- Yang LW, Cui JW, Zhang TJ, Lin GL (2021) Analysis of near-field strong motion characteristics of the Yangbi M6.4 earthquake in Yunnan province in 2021. *World Earthq Eng* 37(4):81–90 (In Chinese)
- Zafarani H, Rahimi M, Noorzad A, Hassani B, Khazaei B (2015) Stochastic simulation of strong-motion records from the 2012 Ahar-Varzaghan Dual earthquakes, Northwest of Iran. *Bull Seismol Soc Am* 105(3):1419–1434
- Zhang KL, Gan WJ, Liang SM, Xiao GR, Dai CL, Wang YB, Li ZJ, Zhang L, Ma GQ (2021) Coseismic displacement and slip distribution of the 2021 May 21, Ms 6.4, Yangbi earthquake derived from GNSS observations. *Chin J Geophys* 64(7):2253–2266 (in Chinese)
- Zhang LB, Fu L, Liu AW, Chen S (2023) Simulating the strong ground motion of the 2022 Ms 6.8 Luding earthquakes, Sichuan, China. *Earthq Sci* 36(4):283–296
- Zhou H, Li YN, Chang Y (2021) Simulation and analysis of spatial distribution characteristics of strong ground motions by the 2021 Yangbi, Yunnan province Ms6.4 earthquake. *Chin J Geophys* 64(12):4536–4537. <https://doi.org/10.6038/cjg2021P0421> (In Chinese)

Publisher's Note Springer Nature remains neutral with regard to jurisdictional claims in published maps and institutional affiliations.

Springer Nature or its licensor (e.g. a society or other partner) holds exclusive rights to this article under a publishing agreement with the author(s) or other rightsholder(s); author self-archiving of the accepted manuscript version of this article is solely governed by the terms of such publishing agreement and applicable law.